All-Atom Molecular Dynamics Simulations of β-Hairpins Stabilized by a Tight Turn: Pronounced Heterogeneous Folding Pathways

Joohyun Kim[†] and Timothy A. Keiderling*

Department of Chemistry, University of Illinois at Chicago, 845 West Taylor Street (M/C 111), Chicago, Illinois 60607-7061

Received: December 24, 2009; Revised Manuscript Received: May 18, 2010

Formation of β-hairpins for a series of peptides having the same general sequence, RYVEV-XG-KKILQ-NH_2, where the $i + 1$th residue, X, at the β-turn is varied (Aib or B in BG12, ^{D}Pro or ^{D}P in ^{D}PG12, ^{L}Pro or P in PG12, and Asn or N in NG12) was studied by means of all-atom Molecular Dynamics (MD) simulations. Trajectories of the tryptophan zipper β-hairpin peptide, TZ2 (SWTWE-NG-KWTWK), were also run under similar conditions to provide a comparison with results for a like-sized peptide with a different characteristic folding mechanism. Four-residue peptides with a sequence, X-BG-K-NH_2 (where X is a V or ^{D}V) were further simulated, particularly focusing on the mirror turn propensity in these hairpins. Microscopic bases for several previous experimental observations are clearly indicated in our MD trajectories. Our results suggest that the two Gellman hairpins, BG12 and ^{D}PG12, have stabilities with a pronounced contribution from the tight turn and a moderate contribution from the cross-strand interactions, resulting in a complicated interplay between turn and strand, while TZ2 appears to undergo simpler (un)folding, dominated by cross-strand interactions. Such an interplay between the turn and the strand observed with BG12 and ^{D}PG12 may underlie their heterogeneous folding dynamics and the absence of a sigmoidal transition in their thermal unfolding profiles determined with IR spectra, as has been shown in previous experimental studies.

I. Introduction

Studies in protein folding have addressed the question of how information encoded in just the sequence of amino acids can dictate three-dimensional self-organization or misfolding. Microscopic details of folding pathways are needed for elucidating the folding mechanism, but these have been developed for only a few peptides or proteins. The size of a system can be an obstacle since available techniques are not always practical for large systems. Instead, studying small proteins or peptides composed of a minimal number of secondary structure motifs seems to be a viable alternative strategy, and indeed many studies have successfully probed atomistic details of the folding mechanisms of small peptides, including de novo designed ones.[2−11] The mechanism of secondary structure formation, particularly for β-hairpins or α-helices, has been actively targeted since results are not only informative for secondary structures themselves but also relevant to the initial steps in some protein folding mechanisms and those of complex proteins in general.[2,7,9,10,12−17]

Vibrational spectroscopy has played a significant role for biophysical characterization of the formation of α-helices and β-hairpins, and isotope-edited IR has further provided site-specific structural information at a residue level, with the potential of studying dynamics with very fast time resolution.[1,18−27] Interpretation of such data has been enhanced by Density Functional Theory (DFT) calculations of force fields and intensities to simulate ^{13}C isotope-edited amide I spectra.[19,20,28−32] Motivated by such successes, study of the impact of conformational dynamics on spectra by employing MD simulations becomes the next challenge. We previously showed that sampling representative conformations from MD trajectories provided better agreement of DFT and experimental spectra as well as more physical insights into the unfolding process.[19] Here we continue efforts to understand β-hairpin formation as stabilized with tight turns, such as by Aib-Gly or ^{D}Pro-Gly, via analyses of the MD trajectories computed under various conditions.

While secondary structure formation of helices has been the focus of intense study and a consensus on central issues related to their folding mechanism has emerged, studies on sheet models are less developed. One problem was the design of models for sheet structures that are stable in aqueous solution, which requires balancing sufficient solubility with the need for interstrand hydrophobic interactions to enable strand collapse and formation of interstrand H-bond formation. The β-hairpin structure, comprising a β-turn and a simple two-strand antiparallel β-sheet, is a minimal model for understanding β-sheet formation, and many β-sheet or β-hairpin models that successfully fold into sheetlike structures in solution are now known.[2,5,9,10,14,19,20,33−43] β-Hairpin motifs were also recently investigated for the design of nucleotide receptor recognition or for drug discovery strategies that pursue inhibition of protein−protein or protein−nucleic acid interactions.[44,45]

A series of 12-residue peptides that form hairpins were initially designed with variants of the sequence RYVEV-^{D}PG-KKILQ-NH_2 by Gellman and co-workers[46,47] where the ^{D}Pro-Gly sequence, here designated ^{D}PG12, forms a tight turn that aligns well with the dominant sense of twist found in β-sheet strands. Subsequently, we have studied ^{D}PG12 and variants of this sequence, NG12, in which Asn is substituted, and BG12, in which ^{D}Pro is replaced with Aib (α-amino isobutyric residue).[1,8,13,18,19] These were chosen since an Aib-Gly sequence (BG12) has a propensity for a tight β-turn,[48,49] and Asn-Gly

* To whom correspondence should be addressed. E-mail: tak@uic.edu.
[†] Current address: Center for Computation and Technology, Louisiana State University, 216 Johnston Hall, Baton Rouge, LA 70803. E-mail: jhkim@cct.lsu.edu.

10.1021/jp912159t
Published on Web 06/09/2010

sequences (NG12) have a high incidence in tight turns found in structurally characterized proteins. The experimental findings from CD as well as IR spectroscopy suggested that the folded state of these peptides has quite different stabilities, with ^{D}PG12 and BG12 forming good β-hairpins but NG12 only a poor one, and PG12 does not form a hairpin.[1,18,46] For comparison, we also simulated under similar conditions unfolding of one of Cochran and co-workers' tryptophan zippers, SWTWE-NG-KWTWK, or TZ2, which has a very stable β-hairpin fold.[6,24,32,39,40] TZ2 shows a sigmodal thermal transition, but ^{D}PG12 and BG12 lack such behavior.[1,23,24,30] NG12 and TZ2 both have an Asn-Gly turn sequence yet still have a significant difference in folding stability.

In this work, our key goal was to elucidate origins of experimental observations for the turn sequence dependence of folding and structure characteristics of the Gellman sequence peptides, BG12, ^{D}PG12, and NG12, and contrast them to properties for TZ2 and PG12, through all-atom MD simulations.[5,6,8,13,23,35,49,50] The paper is organized as follows. Simulation details are presented in Section II, simulation results and analysis focusing on atomistic details in Section III, including insight regarding questions arising from experimental findings, and discussions and conclusions in Sections IV and V, respectively.

II. Simulation Details

Peptide Systems. Reflecting the sequence designs used to collect experimental data, the simulations were done for 12-mer hairpin peptides having the C-terminus blocked with $-NH_2$ and the N-terminus unblocked,[1,8,13] and the tetrapeptides are modeled with CH_3CO blocking the N-terminus, as indicated schematically in Figure 1. The five cross-strand H-bond distances, H_A-H_E, which we use as key quantities for monitoring conformational dynamics as well as stability along the trajectories, are indicated.

Explicit Water MD Simulation. All MD simulations were carried out using the Gromacs v3.2 and v3.3 packages.[51] The OPLS-AA force field was used for the peptides as well as for counterions, Cl^-, required for neutralization, and the SPC model was used for water molecules.[52] The leapfrog integrator was used, and a time step was set to 2 fs. The LINCS algorithm was employed for constraining all equilibrium bond distances. Our simulation box for 12-residue hairpin models was initially prepared to be about 3.0 nm along each side, and about 1000−1500 water molecules were added to solvate the peptide system. Appropriate numbers of counterions were added for charge neutralization. The final rectangular box size was determined by an NPT run at 1 atm. The production trajectories were obtained under NVT or NPT. For temperature control, the Berendsen thermostat was used with a coupling time of 0.1 ps, and for pressure control, the Berendsen scheme was used with a 0.5 ps time constant. For the tetrapeptide models, BG4 and BG4-^{D}Val, smaller simulation boxes were created that contain about 500 waters. A periodic boundary condition was imposed, and the electrostatic long-range interactions were implemented with the Particle Mesh Ewald (PME) method or a simple cutoff. The latter was only used for some of "the long-time trajectories" to increase the total length of a simulation run. The cut-offs were set to 1.0 or 1.2 nm, and we did not find any significant difference between runs using cut-offs and runs using PME in terms of conformational dynamics.

Briefly, the overall procedure for preparing simulations is as follows. An initial conformation for ^{D}PG12, BG12, and TZ2 was chosen from reported NMR-derived structures,[6,49,53] and for NG12, the NMR structure of ^{D}PG12 was modified by mutating ^{D}Pro with Asn using PyMOL.[54] The peptide structure was then transferred to the solvent-filled box, and counterions were added using modules in the Gromacs packages. A minimization step was applied to avoid bad contacts possibly created in the system construction, and the system was heated to temperatures of interest in several steps. At a target temperature, first an initial NPT simulation was run over 1 ns, and then a production trajectory was computed with NVT or NPT ensemble simulations.

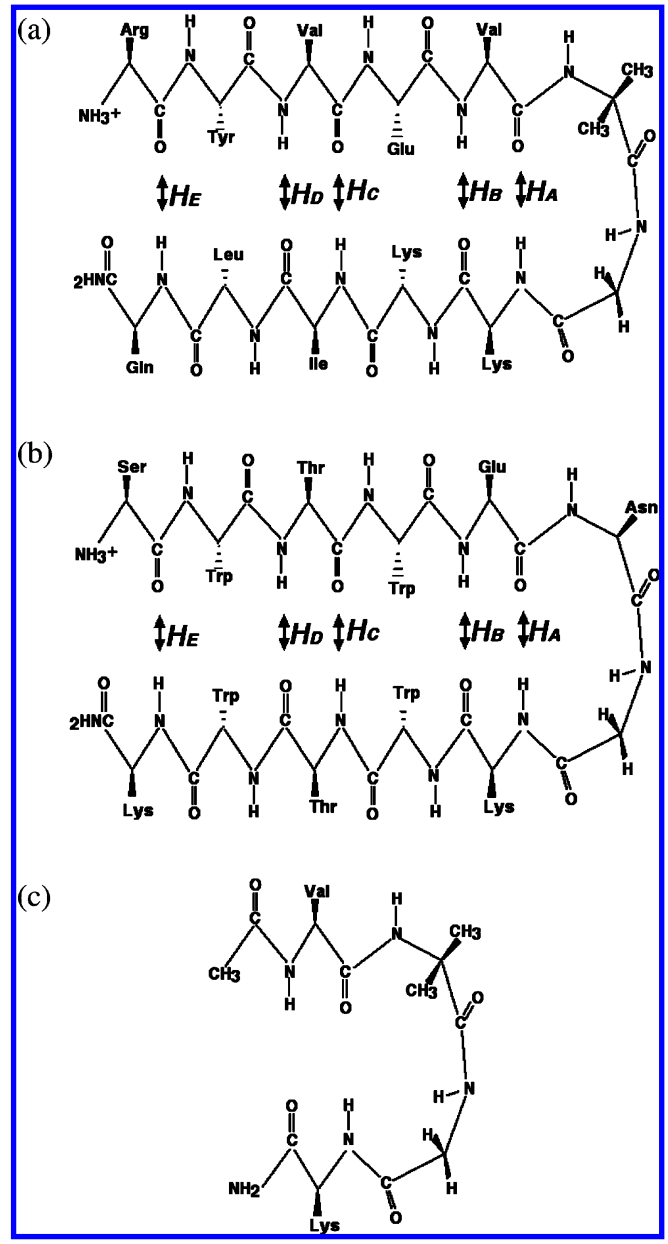

Figure 1. Schematic representation of the β-hairpin models studied in the work with MD simulations. In (a), BG12 is illustrated. Three other Gellman hairpin models, ^{D}PG12, NG12, and PG12, have the same sequence except the $i+1$th residue at the β-turn with ^{D}Pro, Asn, and Pro instead of Aib, respectively. In (b), TZ2, a Tryptophan zipper β-hairpin, is shown. For the 12-mer hairpins, five native H-bonds observed in NMR structures are illustrated. In (c), the tetrapeptide models with the sequence X-BG-K is illustrated. Two variants, BG4 and BG4-^{D}Val, are different in the ith residue, X, such that the former has Val and the latter has ^{D}Val at the position.

Our MD trajectories for the 12-residue hairpins can be grouped into two types. The first group of trajectories comprises conventional *straightforward simulations* producing relatively long time trajectories typically reaching 100 ns and thereby

TABLE 1: Summary of Trajectories with the Straightforward Simulations

peptide	sim. ID	length (ns)	T (K)	trajectory description[a]
BG12	BG12-I	20	300	9 (W-F) − 11 (U)
	BG12-II	100	350	42 (U) − 24 (P-F) − 34 (U)
	BG12-III	50	350	16 (U) − 15 (P-F) − 19 (U)
	BG12-IV	100	300	81 (U) − 10 (P-F) − 9 (U)
	BG12-V	100	280	58 (P-F) − 2 (W-F) − 45 (U)
	BG12-VI	100	280	5 (P-F) − 95 (U)
	BG12-S1	250	310	50 (P-F) − 130 (U) − 20 (P-F)
^{D}PG12	^{D}PG12-I	100	350	5 (W-F) − 60 (U) − 35 (P-F)
	^{D}PG12-II	100	350	2 (P-F) − 94 (U) − 4 (P-F)
	^{D}PG12-III	50	400	1 (P-F) − 29 (U) − 6 (P-F) − 2 (U) − 9 (P-F) − 3 (U)
	^{D}PG12-IV	50	280	18 (P-F) − 18 (U) − 6 (P-F) − 8 (U)
	^{D}PG12-S2	300	310	140 (P-F) − 160 (U)
NG12	NG12-I	100	350	9 (W-F) − 60 (U) − 7 (P-F) − 24 (U)
	NG12-II	10	400	5 (W-F) − 5 (U)
	NG12-III	20	450	1 (W-F) − 19 (U)
TZ2	TZ2-I	100	400	5 (P-F) − 85 (U) − 5 (P-F) − 5 (U)
	TZ2-II	100	350	100 (W-F)
	TZ2-III	100	280	37 (W-F) − 15 (P-F) − 48 (U)
	TZ2-IV	50	350	6 (P-F) − 44 (U)
	TZ2-V	100	400	16 (U) − 9 (P-F) − 45 (U) − 10 (P-F) − 4 (U) − 7 (P-F) − 9 (U)
	TZ2-VI	50	500	5 (P-F) − 45 (U) − 5 (P-F)
	TZ2-VII	100	350	100 (U)

[a] Each trajectory is described with respect to the occurrence of three states, W-F, P-F, and U, along the trajectory. The number represents the duration time of the state in nanoseconds, and the identified state is described in the following parentheses. W-F, P-F, and U are defined in the text.

generating many unfolding and refolding events. These were run at a variety of temperatures (as indicated in Table 1) to broaden the simulated behaviors. In addition, two much longer trajectories for BG12 and ^{D}PG12 starting from partially folded structures and reaching 250 and 300 ns were run at 310 K (BG12-S1 and ^{D}PG12-S2) as summarized in the Supporting Information, Figures S1 and S2.

In Table 1, those trajectories are summarized, in particular, with respect to transitions between conformers that can be identified as Well-Folded (W-F), Partially-Folded (P-F), and Unfolded (U) states. The W-F represents a well-folded conformation with four established H-bonds at H_A, H_B, H_C, and H_D, while the P-F represents partially folded structures having H-bonds at H_A, H_B, and H_C and the U state the unfolded state.

The second group of trajectories, on the other hand, can be termed *unfolding simulations* designed to scrutinize unfolding pathways inspired by a stochastic simulation for the measurement of the mean first passage time and the rate constant.[55,56] For this scheme, we sample a set of configurations representing the ensemble of the W-F state that is subsequently used for initial configurations of multiple unfolding simulations. First, an independent 5 ns trajectory was obtained at 300 K under NPT conditions starting from an NMR-based structure. Then, during this NPT run, ten folded conformations were derived by capturing the structure at every 500 ps. The unfolding simulations using these conformations were carried out at high temperature, 450 K, because at lower temperatures we had difficulty in observing an unfolding event, in that a number of them did not unfold in a practical time frame. It is noted that the dump interval for these unfolding simulations should be smaller than for the straightforward simulations, ensuring that any conformational fluctuation should be identified (see Supporting Information, Table S-I).

To study implications of the turn handedness, simulations with PG12 were carried out at 300 and 450 K starting from the ^{D}PG12 NMR structure but with ^{D}Pro replaced by ^{L}Pro. Simulations of tetrapeptide models, BG4 and BG4-^{D}Val, were also carried out at 300 and 450 K, starting from an initial conformation derived from the NMR structure of BG12.

In this work, trajectories were obtained with three different systems using a serial version of Gromacs. When we used a machine equipped with a 2.8 GHz Intel Xeon processor, we were capable of producing a 2 ns trajectory in about 24 h for a system comprising a 12-mer peptide with PME.

Trajectory Analysis. Obtained trajectories were analyzed with programs provided by Gromacs as well as by use of python scripts we wrote for this study. Principal component analysis (PCA) applied to the covariance matrix was used to characterize the unfolding pathway. The covariance matrix was constructed for backbone atoms using the nonmass-weighted coordinates, and it was diagonalized, using modules in Gromacs packages.[51,57]

With *unfolding simulations*, the unfolding pathways as well as an unfolding time, represented as the First Escape Time (FET), were obtained by monitoring the five H-bond distances. A broken H-bond is assessed as having an H-bond distance greater than 0.4 nm between a donor N and an acceptor O. This distance is much longer than the standard criterion for the formation of H-bond, but we intentionally chose it to avoid complications arising from recrossing dynamics or border dynamics.[58] The N−H−O angle criterion is not applied since the distance criterion is sufficient to detect the H-bond disruption. We slightly overestimate the FET, but since the FET time scale is well separated from that of a relatively fast transition event (see below), this has little impact on FET analyses.

III. Results

Long-Time Trajectories from Straightforward Simulations. We obtained trajectories of *long-time straightforward simulations* up to 300 ns. With this time scale and the range of temperatures for the simulations, the trajectories display unfolding events from the initial folded state (designated as W-F) to an unfolded state (U) as well as to partially folded states (P-F) that emerge from the refolding dynamics (see Table 1).

An immediate observation was that the folded conformations of BG12, ^{D}PG12, and TZ2 were substantially stable. Simulations carried out at temperatures below 350 K did not easily produce an unfolding event. Unlike the other hairpins, according to our obtained trajectories, the folded state of NG12 is apparently not stable since an unfolding event appears quickly. One caveat is that the initial conformation of NG12 was constructed from the NMR structure of ^{D}PG12. However, experimentally, NG12 is known to be a weak folder, forming only a partial hairpin in water under normal conditions,[13,46] and the computed conformational dynamics characteristics further support this (see below).

Three distinguishable states, W-F, P-F, and U, are observed in all β-hairpin models, as identified by cross-strand H-bonds, but the P-F state in NG12 has relatively short duration (Table 1). While the transitions from one state to another are quick and not immediately reversed, we require that a state be maintained for many nanoseconds to be observed. Among three states, W-F is found when a trajectory starts from an NMR-derived conformation before an unfolding transition to the U state. On the other hand, the P−F state was observed when a refolding pathway from the U state successfully resulted in a hairpin-like structure composed of a turn structure but only a partially formed β-strand structure. P−F is indicated to be a distinguishable intermediate state, different from U or W-F, by the observation that its conformational character is defined

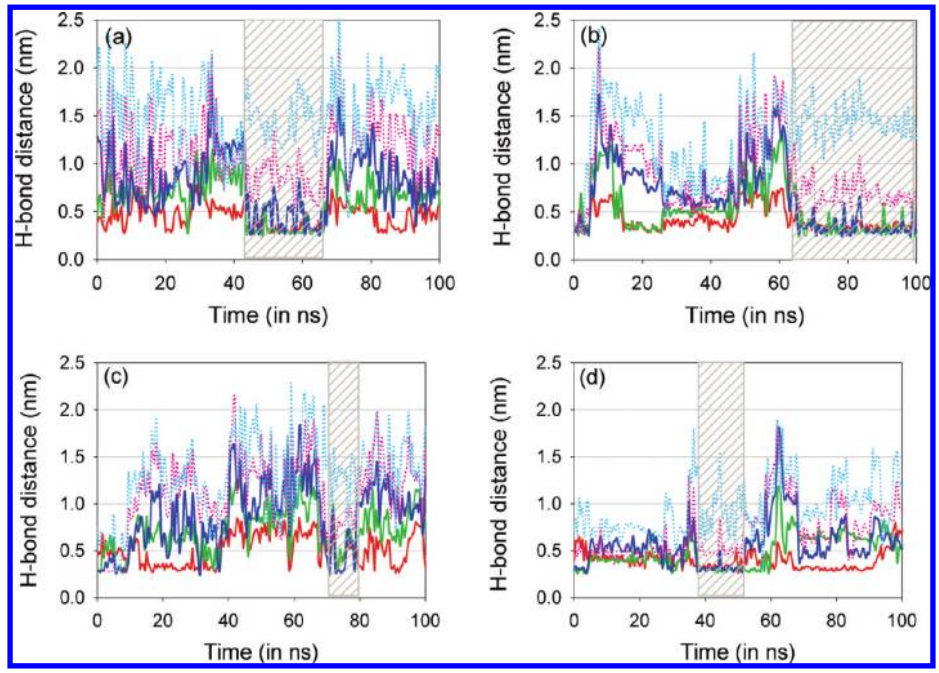

Figure 2. Conformational dynamics indicating a potential role of the turn sequence in refolding dynamics. Conformational dynamics around a refolding event to the P-F are compared for the four 12-mer hairpins with respect to five H-bond distances, H_A (solid red), H_B (solid green), H_C (solid blue), H_D (dotted pink), and H_E (dotted cyan). (a) A part of the trajectory of BG12-II. (b) A part of the trajectory of ^{D}PG12-I. (c) A part of the trajectory of NG12-I. (d) A part of the trajectory of TZ2-III. The P-F state is emphasized with a shadowed box.

in terms of H-bond formation that lasts over many nanoseconds, in contrast to transient species behavior. For example, the BG12-II trajectory has a 24 ns period for the P-F state followed by 42 ns for the unfolded state.

Our results do not give evidence for the reappearance of the fully folded W-F state along a trajectory after formation of U or P-F states (except for a short-lived, 2 ns metastable state in BG12-VI). Presumably, the time scale of simulation is still not long enough to reach the level where complete statistical refolding dynamics to W-F can be observed.[59−62] In fact, we simulated two long trajectories at 310 K for BG12 (BG12-S1) and ^{D}PG12 (^{D}PG12-S2) that started from P-F configurations (see Supporting Information Figures S1 and S2) and reached 250 and 300 ns, but no evidence was found for subsequent folding into the W-F state in this time scale. According to previous MD simulation studies of TZ2, when an explicit water model was used, absences or difficulty of refolding dynamics resulting in the W−F state were reported.[50,62−64] Note that with an implicit water model refolding events into the W-F state were reported with simulations utilizing distributed computing resources via the folding@home project.[5]

To examine the possibility of refolding to the W-F from the P-F and thus to evaluate the relevance of the P-F state as an intermediate along a refolding pathway back to the W-F, we carried out some specially managed simulations, BG12-V and BG12-VI, at lower temperatures. Starting from the same initial P-F configuration, these ended in the U rather than the W-F state, which, in addition to the results of BG12-S1, suggests that the free energy barrier from the P-F to the W-F is higher than to the U state.

NG12, a Weak β-Hairpin Folder, Role of the Asn-Gly Turn. According to previous experimental results, NG12 appears to be a weak β-hairpin folder, and compelling evidence for this was also found in the refolding dynamics. In Figure 2 and Figure 3, we compare conformational dynamics of four 12-mer hairpins. Trajectories are taken from BG12-II, ^{D}PG12-I, NG12-I, and TZ2-III (see Table 1). In each case, the time frame displayed encompasses a period of the P-F state that occurs after a period of the U state, showing comparative refolding dynamics. Overall conformational fluctuations are tracked with five H-bond distances (Figure 2) as well as backbone torsion angles of the turn residue at $i + 1$. (Figure 3). In the P-F states, two broken H-bonds at H_D and H_E have distances in sharp contrast to the three relatively stable H-bonds close to the turn.

The P-F duration for NG12 is the shortest among these four hairpins (Figure 3). The ^{D}Pro-Gly turn (Figure 3(b)) and the Aib-Gly turn (Figure 3(a)) easily adopt ideal β-turn geometries during a refolding event, which shows the nascent turn geometry to be stable and a promoter of a P-F structure. In both cases, the ϕ angles at $i + 1$th residues are very tightly distributed around the target value, ~60°, characteristic of the ideal mirror turn (I′, II′, or III′) geometries,.[65] The ^{D}Pro-Gly adopts two distinct distributions for ψ, close to either 30° or −120°, suggesting that these turns can choose Type I′ or Type II′ forms, respectively. By contrast, the Aib-Gly (Figure 3(a)) turn in BG12 strongly favors ψ~30° and thus forms Type I′ turns in the P-F structure. Note that such dihedral angle distributions are in good agreement with previous X-ray or NMR structure determinations.[46,47,49] By contrast, dihedral angles of the Asn residue in NG12 (Figure 3c) were found with values of ϕ in the range of −50° ~ −150°, indicating that the mirror turn types, which favor β-hairpin structure, are not easily achieved without energetic balancing from other factors such as interactions between strands. Therefore, the turn of NG12 will not be a deciding factor for hairpin formation. TZ2 (Figure 3(d)), comprising an Asn-Gly turn, showed a dynamical adjustment of the backbone dihedral angles from a common to a mirror form, approximating a Type I′ turn, after the transition into the P-F state began (Figure 3d, ~40 ns).

Conformational Fluctuation during the W-F and the P-F States. Stability was further analyzed by comparing conformational fluctuations among folded hairpins with sampled structures obtained during periods characterized by formation of W-F and

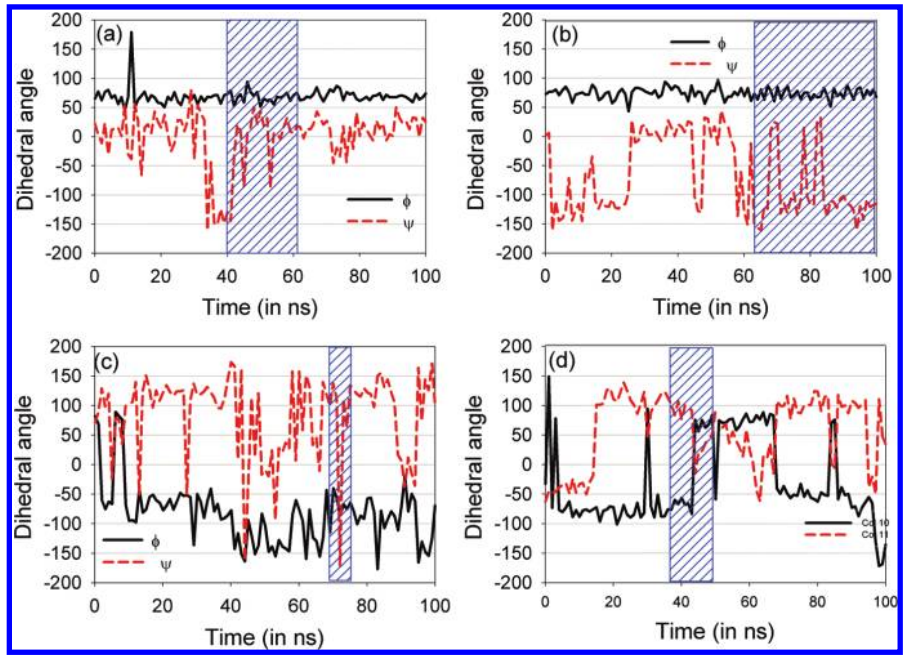

Figure 3. Conformational dynamics indicating a potential role of the turn sequence in refolding dynamics. The same trajectories shown in Figure 2 are illustrated here with respect to the two dihedral angles (ϕ and ψ) of the $i + 1$th residue of the β-turn.

TABLE 2: Comparison of Conformational Fluctuation among the 12-mer Hairpins[a]

	sampling condition							
hairpin model	temp (K)	time (ns)	state	H_A (nm)	H_B (nm)	H_C (nm)	H_D (nm)	H_E (nm)
BG12	300	5	W-F	0.34 (0.04)	0.29 (0.02)	0.30 (0.02)	0.29 (0.01)	0.31 (0.06)
	350	5	W-F	0.34 (0.05)	0.29 (0.02)	0.30 (0.02)	0.30 (0.02)	0.31 (0.05)
	350	20	P-F	0.35 (0.06)	0.31 (0.058)	0.43 (0.16)	0.84 (0.19)	1.42 (0.21)
		NMR[b]		**0.32**	**0.33**	**0.26**	**0.25**	**0.25**
[D]PG12	350	5	W-F	0.33 (0.04)	0.31 (0.05)	0.30 (0.02)	0.30 (0.02)	0.33 (0.06)
	400	16	W-F	0.33 (0.03)	0.30 (0.03)	0.30 (0.03)	0.30 (0.02)	0.33 (0.08)
	450	9.5	W-F	0.34 (0.04)	0.31 (0.05)	0.30 (0.03)	0.31 (0.06)	0.40 (0.19)
	450	9.5	W-F	0.34 (0.04)	0.31 (0.04)	0.33 (0.08)	0.40 (0.16)	0.60 (0.34)
	350	30	P-F	0.35 (0.05)	0.33 (0.08)	0.34 (0.09)	0.68 (0.11)	1.45 (0.15)
	350	2	P-F	0.33 (0.03)	0.30 (0.04)	0.31 (0.002)	0.57 (0.002)	1.27 (0.13)
		NMR[c]		**0.27 (0.008)**	**0.32 (0.03)**	**0.34 (0.04)**	**0.34 (0.04)**	**0.48 (0.08)**
NG12	350	5	W-F	0.49 (0.07)	0.41 (0.14)	0.34 (0.06)	0.30 (0.03)	0.52 (0.15)
TZ2	400	20	W-F	0.36 (0.06)	0.29 (0.02)	0.29 (0.02)	0.29 (0.02)	0.33 (0.07)
	450	10	W-F	0.36 (0.07)	0.29 (0.02)	0.29 (0.02)	0.29 (0.02)	0.33 (0.10)
	300	3.3	P-F	0.35 (0.03)	0.30 (0.02)	0.33 (0.04)	0.46 (0.04)	0.84 (0.21)
	350	7	P-F	0.38 (0.07)	0.29 (0.02)	0.32 (0.06)	0.52 (0.12)	0.84 (0.21)
	350	3.7	P-F	0.35 (0.04)	0.30 (0.02)	0.32 (0.04)	0.43 (0.03)	0.65 (0.07)
		NMR[d]		**0.29 (0.012)**	**0.28 (0.007)**	**0.28 (0.012)**	**0.28 (0.012)**	**0.30 (0.012)**

[a] The distribution of five cross-strand H-bond distances is measured with the mean and the standard deviation values. Conformations are obtained during the period of the W-F or P-F state. For comparison, values calculated from NMR structures are also presented. [b] 1 NMR structure (unpublished data from R. P. Hammer). [c] 20 NMR structures (data from S. Gellman, personal communication). [d] 20 NMR structures (PDB id: 1LE1).[6]

P-F states. In Table 2, the mean values and standard deviations for the five cross-strand H-bonds are compared. Where available, conformational variations that can be observed among the best NMR-determined structures (obtained at somewhat lower temperatures to access stable structures) are also listed for comparison to our trajectory results. Regardless of hairpin models, the amount of fraying in the strand termination region differentiates the two folded states, W-F and P-F. The P-F state comprises structures with two broken H-bonds, H_D and H_E. Among NMR structures, apparently, conformations belonging to P-F are absent, and less conformational fluctuations in the turn region are indicated.

According to our simulations, the Gellman hairpins had slightly larger mean values for the H-bond distances at H_C as compared with TZ2, and a more pronounced difference is found when conformations from P-F are compared, which indicates that the stronger cross-strand hydrophobic interactions in TZ2 maintain shorter H-bond distances. By contrast, the Asn-Gly turn in TZ2 yields larger fluctuations for H_A compared to both the Aib-Gly turn in BG12 and the [D]Pro-Gly turn in [D]PG12. Our recent NMR structural results also found evidence for fluctuations in the turn of TZ2.[24] For those folded conformations seen in the NG12 trajectories, i.e., NG12-I, NG12-II, and NG12-III, the average H-bond distance at H_A is ~0.5 nm, which is much larger than found for TZ2, which also has an Asn-Gly turn. The absence of unique strong cross-strand hydrophobic interactions in NG12 appears to result in a destabilization of the turn as witnessed by a larger mean value of H_A than for TZ2. Finally, the tight turns in [D]PG12 and BG12, stabilized by those

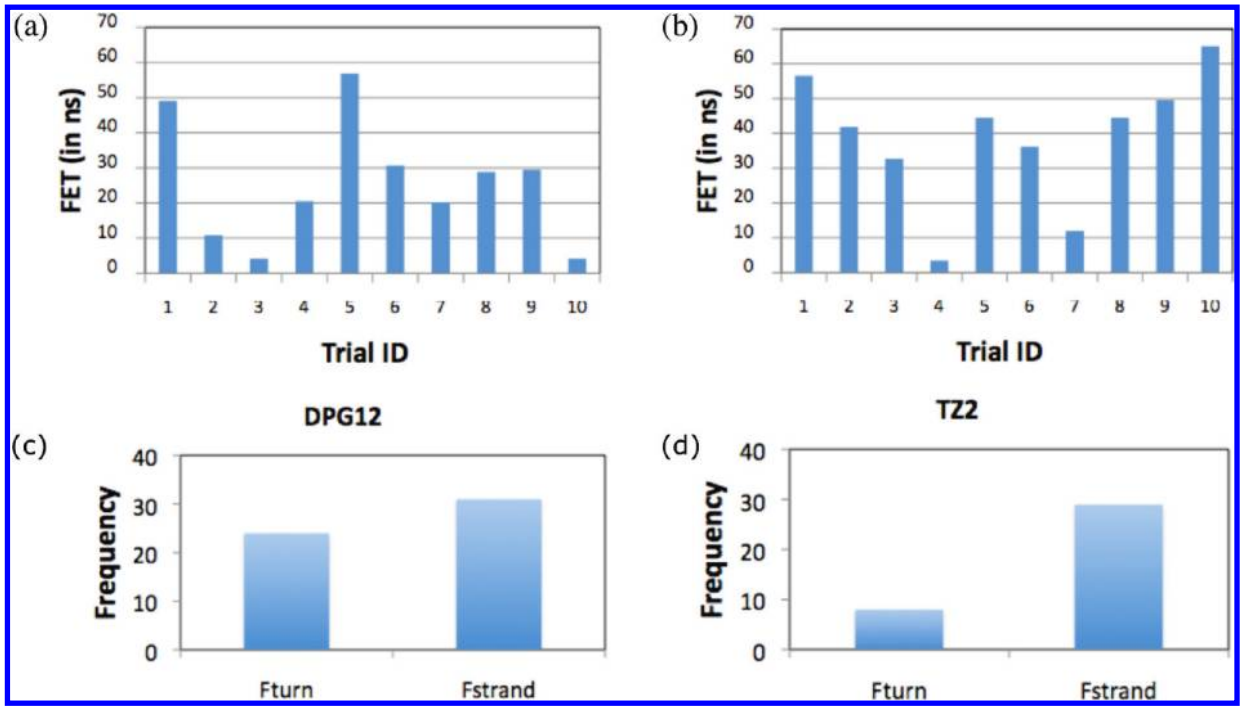

Figure 4. Summary of the unfolding simulation results. The measured First Escape Time (FET) of 10 trajectories is shown in (a) and (b) for ^{D}PG12 and TZ2, respectively. In (c) and (d), the frequency of occurrence of the short-lived kinetic intermediates, F_{turn} and F_{strand}, observed along a unfolding trajectory as counted for ^{D}PG12 and TZ2, respectively, are presented.

sequences,[1,9] result in a smaller mean value of H_A than found in the NG12 models.

Unfolding Simulations: Characteristic Differences Between ^{D}PG12 and TZ2. A comparative investigation of unfolding dynamics for TZ2 and ^{D}PG12 was conducted by simulating their *unfolding trajectories*. The simulation of these trajectories was designed to sample unfolding pathways efficiently. Stochastic simulations have been used for estimating the average of the First Passage Time, or the Mean First Passage Time (MFPT), from one state to another state by carrying out multiple simulations starting from an initial configuration representing the W-F equilibrium state.[56,66] With the unfolding trajectories, we could similarly obtain the First Escape Time (FET) for each trajectory when the escape from the initial W-F state is irreversibly completed, breaking all four H-bond distances, H_A-H_D, for the first time. H_E was not considered since its pronounced fraying is highly uncorrelated with overall escape dynamics in the temperature range of interest. Our results, shown in Figure 4(a) and (b), yield mean FETs (standard deviation in parentheses) of 38.7 ns (18.9 ns) and 25.5 ns (17.6 ns) for TZ2 and ^{D}PG12, respectively.

Due to high computational cost of an all-atom simulation with explicit water, the total number of our simulations used was limited to 10, and as a result the mean FET has significant error so that their differences are not statistically significant. Nonetheless, each unfolding trajectory contains a variety of conformational dynamical events corresponding to a relevant part of the rugged potential energy landscape. The detailed dynamics are summarized in the Supporting Information, Table S-I. Figure 4(c) and (d) summarize the statistics of conformational fluctuations in terms of the occurrence of kinetic intermediates described below.

With the observations from the *straightforward simulations*, it became clear to us that an unfolding pathway can be characterized by detecting the occurrence of four kinetic intermediates, P-F, P-F*, F_{turn}, and F_{strand}. F_{strand} represents a short-lived state with only two H-bonds, at H_C and H_D, and F_{turn} also has only two H-bonds, but at the turn region, H_A and H_B. Whereas F_{turn} and F_{strand} are very short-lived intermediates, the states P-F and P-F* both have three H-bonds and tend to have longer lifetimes. The structural characteristics of the P-F intermediate are the same as those of the P-F state, hence the same notation is applied. P-F* represents those structures having H-bonds at the termini, H_C, H_D, and H_E, but broken at the turn, H_A and H_B, and was previously reported for TZ2[50] but in our results is rare (Run 9 of TZ2).

Some common features from the ^{D}PG12 and TZ2 hairpins include unfolding trajectories that are characterized by numerous failed attempts to unfold, indicating complex escape dynamics, with a final transition to U that occurs in a short time scale as compared to the overall FET. However, the key element of unfolding dynamics of the two hairpin models is frequent occurrences of kinetic intermediates such as F_{turn} and F_{strand}, as summarized in Figure 4(c) and (d) (see also complete details in Table S-I, Supporting Information). Unfolding does not occur in a simple, cooperative breaking event of H_A-H_D, the four dominant H-bonds.

Beyond such commonality, the *unfolding simulations* clearly indicate variations between the ^{D}PG12 and TZ2 β-hairpin models in terms of contributions from the strand and turn regions contributing to stabilization of the folded state. The higher frequency of occurrence of F_{turn} in ^{D}PG12 than for TZ2 in Figure 4(c) and (d) illustrates its role in the mechanism. For example, Run 1 of ^{D}PG12 yields a better-than-average 49 ns FET, in spite of numerous attempts to unfold, as indicated by frequent appearances of F_{turn}. On the other hand, Figure 5(b) illustrates that, contrary to ^{D}PG12, TZ2 shows correlated motion between H_C and H_D but highly fluctuating conformational dynamics associated with H_A and H_B.

We notice that only one ^{D}PG12 trajectory (Run 7) shows the occurrence of P-F as compared to three trajectories (Run 1, Run 7, and Run 8) with TZ2. This is because in TZ2 strong cross-

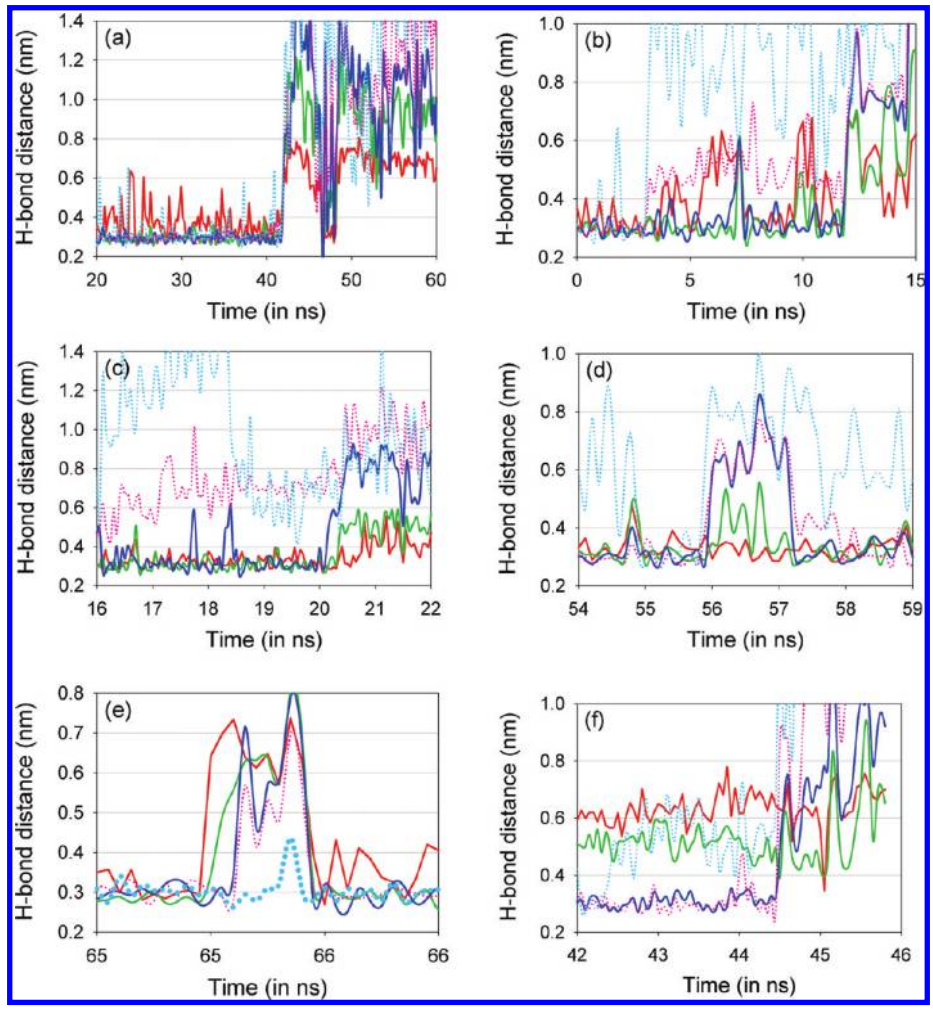

Figure 5. Characteristic features of unfolding trajectories of ^{D}PG12 and TZ2. The coloring scheme for five H-bond distances is consistent with Figure 2. (a) Irreversible cooperative unfolding dynamics breaking H_A-H_D observed in Run 2 of TZ. Similarly, such an unfolding transition is also found in Run 3, Run 4, Run 6, Run 8, Run 9, and Run 10 of ^{D}PG12 and Run 2, Run 3, Run 4, Run 9, and Run 10 of TZ2. (b) Occurrence of the P-F state during unfolding dynamics observed in Run 7 of TZ2. The observation of the P-F is also found in Run 1 and Run 8 of TZ2. (c) Occurrence of the P-F state during unfolding dynamics observed in Run 7 of ^{D}PG12. No other unfolding trajectories of ^{D}PG12 display the P-F state. (d) Example of a role of the turn producing a longer FET with ^{D}PG12. While the residual turn structure resists unfolding, the folded state is retained. This F_{turn} is shown in Run 5 of ^{D}PG12. (e) Example of a role of the strand and an apparent absence of the turn structure with an unfolding trajectory of TZ2, Run 10. (f) Example of an unfolding transition displaying a minimal contribution of the turn. This is observed in Run 5 of TZ2. Note that this unfolding pathway goes through F_{strand}.

strand interactions arising from side-chain hydrophobic interactions among the four tryptophans tend to maintain hydrogen bonds at H_C and H_D, thus unfolding pathways have a greater chance of going through P-F. In contrast, moderate cross-strand interactions in ^{D}PG12 are unlikely to sustain a strand structure without contributions from the turn, resulting in an absence of this intermediate. In Figure 5(e) for TZ2, an unfolding transition initially produces a residual structure in which all four H-bonds at H_A-H_D were destroyed, leaving only a H-bond at H_E, but after 1 ns the entire β-hairpin structure is regained. Such behavior indicates that this was a dynamical fluctuation, counteracted by the hydrophobic collapse of the Trps and the remaining H-bond at H_E, which together avoided completion of the unfolding dynamics and brought the conformation back to the folded state.

Principal Component Analysis (PCA) applied to a covariance matrix of the obtained trajectories was introduced to reveal "essential dynamics" in MD studies[57] by reducing the dimension and providing information on conformational dynamics related to the primary components of the conformational rearrangement. PCA was applied to a part of the trajectories in which the folded state is maintained and before any conformational changes occur related to the final unfolding. This extracts the dominant conformational dynamics along the unfolding pathway. In Figure 6, the three lowest PCA modes of ^{D}PG12 and TZ2 are compared in terms of atomic root-mean-square fluctuation (RMSF) of the atoms along the peptide backbone, three per residue. RMSFs of atoms in the turn residues, the Asn-Gly in TZ2, appear to be distinguishably larger than for residues in the strands, resulting in a sharply peaked shape in the first PCA mode (Figure 6d, see, in particular, atoms for the Asn, positions 16−18). By contrast, for ^{D}PG12, the fifth residue, Glu backbone atoms 10−12, just before the ^{D}Pro-Gly turn, and the eighth residue, Lys atoms 22−24, display relatively lower RMSFs in the first PCA mode. This, along with the second PCA mode having significantly smaller RMSFs for the backbone atoms of the ^{D}Pro residue (located at 16−18), emphasizes the collective motion in the Gellman peptide, which tends to separate the conformational motion of the turn and strand residues.

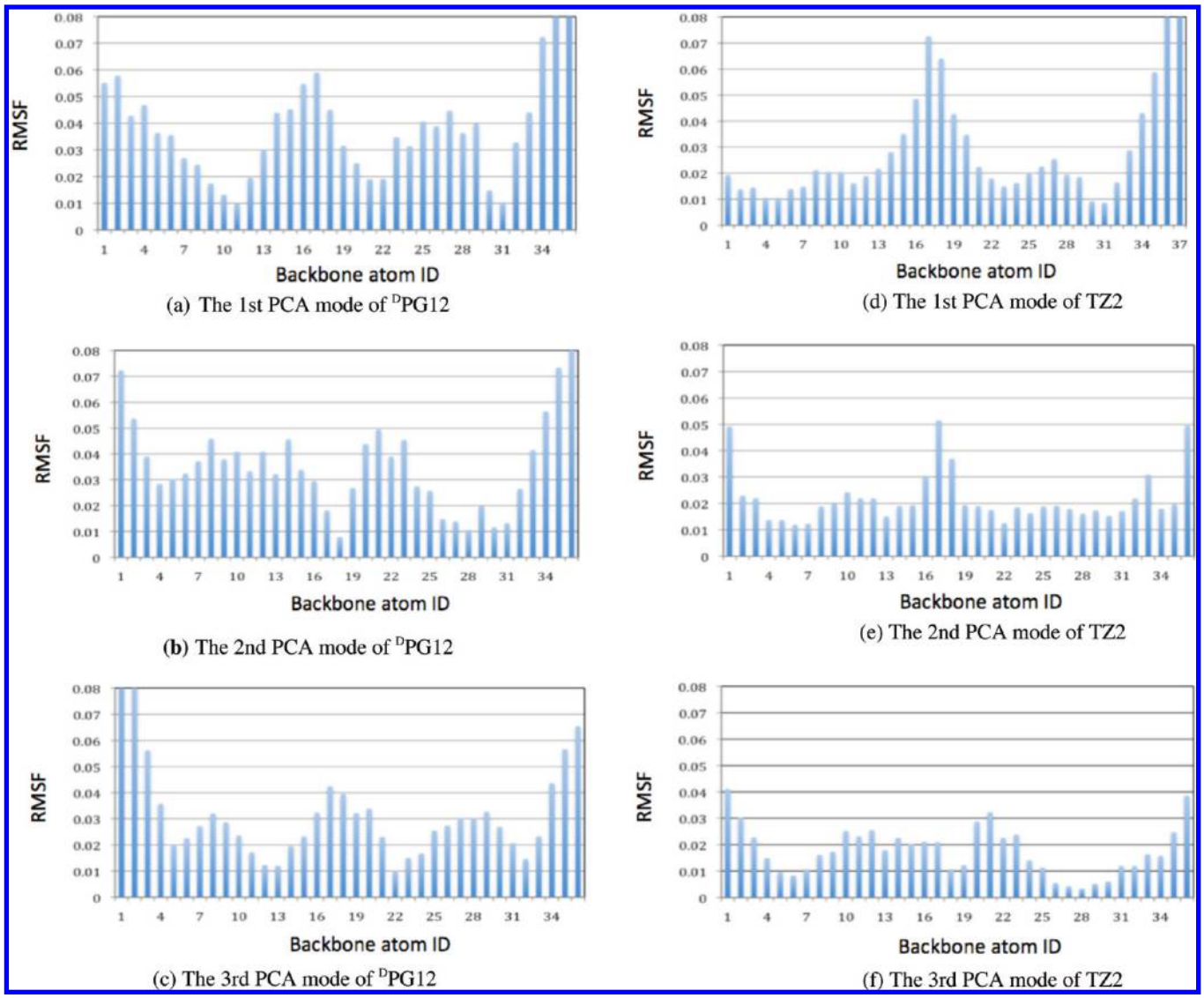

Figure 6. PCA analysis on an unfolding trajectory of ^{D}PG12 and TZ2. In (a), (b), and (c), three PCA modes obtained from the starting 16 ns of Run 5 of ^{D}PG12 are presented. In (d), (e), and (f), three PCA modes from the starting 7 ns of Run 5 of TZ2 are presented. Obtained PCA modes are illustrated with respect to the root-mean-square fluctuation (RMSF) (y axis) for each backbone atom (x axis).

PG12 Simulation: Contrast with the ^{L}Pro-Gly for the β-Turn. Simulations of PG12 were aimed at developing an understanding of the destabilization effect when a turn sequence instead favors the common turn (opposite handedness). In Figure 7, two trajectories obtained with PG12 at 300 and 450 K are displayed, and Figure 7(c) illustrates a part of the trajectory shown in Figure 7(b) again with respect to two backbone angles. Unfolding transitions for PG12 appear sooner as the turn is significantly less stable, in contrast to ^{D}PG12 as can be seen (300 K, Figure 7 (a)). The destabilized turn has larger fluctuations at H_A and H_B during 0−0.5 ns and 1.5−4.8 ns, whereas H_C and H_D are relatively stable. The high temperature run at 450 K shown in Figure 7(b) further confirms that the turn is not likely to contribute in stabilizing a newly formed β-hairpin structure during a refolding attempt since it opens cooperatively with the other bonds. The compelling reason for such a detrimental impact on refolding, as illustrated in Figure 7(c), is that due to the distinctive cyclic side chain of ^{L}Pro the backbone angle ϕ is locked at $\sim -75°$, making the common turn geometry the preferred conformational choice. All refolding attempts observed at 27, 40, and 52 ns in the 450 K trajectory appear to occur via cross-strand interactions, as suggested by the shorter distances of H_C, and notably with H-bond formation at H_D and H_E. Taken together, the impact of ^{D}Pro or ^{L}Pro at the $i + 1$th position in the turn geometry for β-hairpin formation and the importance of ^{D}Pro in the Gellman sequence are clear, as has been addressed empirically by Gellman.[46]

Tetrapeptides, BG4 and BG4-^{D}Val, Simulations: Aib Residue Influence on β-Turn Formation. With BG12, an interesting question is what factors drive an achiral amino acid, such as Aib, to adopt the mirror Type I′ turn ($\phi \approx 60°$, $\psi \approx 30°$) preferentially over the common Type I turn ($\phi \approx -60°$, $\psi \approx -30°$). [It should be noted that Type II or Type II′ turns are unlikely for an Aib-Gly turn sequence due to spatial hindrance.] For this purpose, we additionally simulated two tetrapepide models, BG4 and BG4-^{D}Val. For BG4, a 200 ns run at 300 K and a couple of 100 ns runs at 450 K were carried out, and for BG4-^{D}Val, a 100 ns run at 450 K was carried out. Results are summarized in Table 3.

These trajectories showed frequent transitions between the mirror turn geometry and the common turn geometry. Observed transitions of the turn geometry have also transitions to short-lived extended conformations ($\phi \approx 180°$ or $-180°$), but the major conformational distributions are characterized by ϕ values

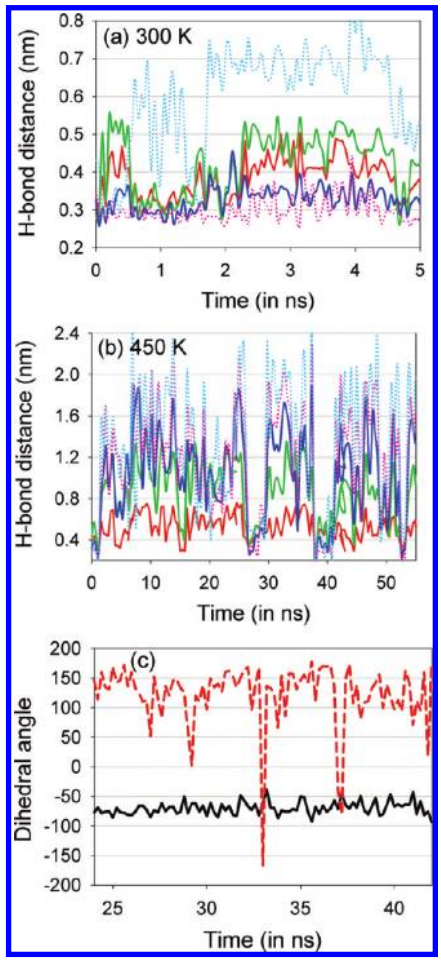

Figure 7. Trajectories of PG12. (a) Trajectory simulated at 300 K is shown. (b) Trajectory simulated at 450 K is shown. The coloring scheme for five H-bond distances is the same as Figure 2. (c) A part of the 450 K run is illustrated with respect to two backbone dihedral angles, ϕ and ψ, of a Pro residue at the $i + 1$th residue of the β-turn.

at the Aib appearing at the common ($\phi \approx -60°$) or the mirror-image ($\phi \approx 60°$) turn geometries. The duration time with the mirror turn values in these trajectories is longer (134 vs 57 ns in 450 K run). Also, we observed that BG4-^{D}Val favored the common turn geometry exclusively (450 K). These results may be understood by that a bulky neighboring residue located at the i-th position, which in this case is Val for BG4 or ^{D}Val for BG4-^{D}Val, favors one type of turn. For example, the ^{L}Val in BG4 having a bulky side chain in the opposite enantiomeric position could disfavor ϕ values of the common turn geometry due to steric hindrance with the Cα-Me groups on Aib.

IV. Discussion

Identification of Three States, W-F, P-F, and U from Conformational Dynamics. Two fundamental issues, force field validation and sampling strategy, pose challenges for molecular dynamics simulations.[59] These challenges have also been recognized in studies of folding for sizable biomolecular systems like proteins and nucleic acids. In particular, the considerable size of the large configuration space corresponding to the unfolded or disordered state contributes to the difficulty in finding an efficient solution for the sampling problem. Our results obtained with *straightforward simulations*, particularly with observation of no return to the W-F state after an unfolding event, are indicative of limited sampling of the configurational space. One refolding to a state similar to W-F (see the trajectory, B12-V in the Table 1) was found; however, this seems to be a transient state reflected in its short, 2 ns lifetime at 280 K, showing it lacks the strong stability otherwise seen for W-F states. We have found that conformational fluctuations, as monitored with H-bond distances as well as torsion angles in the turn, provide a clear picture of transients between W-F, P-F, and U states, giving insight into β-hairpin formation and the different stabilities of each 12-mer hairpin model.

Sampling of Unfolding Pathways with the Unfolding Simulation. Our multiple unfolding simulations were motivated to find an efficient strategy for exploring unfolding pathways. Some supporting arguments for our protocol follow. First, other studies have reported that multiple MD trajectories appear to converge more rapidly than a single long trajectory.[67,68] Second, due to the high entropic barrier from U to W-F, a large part of a trajectory obtained with the straightforward simulations is wasted by being trapped in exploring the unfolded state. Therefore, the investigation of unfolding dynamics is difficult with the straightforward simulations. Less expensive simulation protocols such as coarse-grained models or implicit solvent models might increase the time scale of the total exploration or the number of escapes with the same computing cost, but previous studies and our preliminary data (unpublished) suggest that dynamical folding and unfolding pathways sampled with such protocols would be significantly different from those obtained with all-atom simulations using explicit water.[69]

In this study, the idea of stochastic simulations for the estimation of the Mean First Passage Time (MFPT) and the corresponding rate constant is the basis for the design of unfolding simulations using sampled initial configurations from which the state escapes.[55,56,70] In stochastic simulation approaches, the mean first passage time, τ_{MFPT}, might be estimated by satisfying

$$E(t) = \int_{r\in A} \mathrm{d}r E(t|r) g(r)$$

where

$$\tau_{MFPT} = \int_0^\infty \mathrm{d}t' t' E(t')$$

and $E(t|r)$ represents the escape probability that a system, starting at the configuration, r, escapes from the initial state, A, at time t for the first time. Here, $g(r)$ is the equilibrium distribution. In our scheme, the statistical average of the escape probability over a set of initial configurations is importantly considered for an efficient sampling of unfolding pathways.[56] While each unfolding simulation corresponds to a realization of trials with the probability, $E(t|r)$, the sampling of initial configurations with an equilibrium run implements the integration over the initial state weighted with $g(r)$. Therefore, our unfolding simulation protocol, starting with sampled initial configurations, is expected to explore efficiently the part of the free energy landscape associated with diverse unfolding pathways. While our results are limited by the finite numbers of simulation runs for a quantitative estimation of FET, a variety of unfolding pathways are expected to appear, which is illustrated in the observed dynamics. The comparison of the number of observed intermediates (see Figure 4(c) and (d)) as well as their distributions among unfolding trajectories (see Table S-I, Supporting Information) points to the significant role of the turn in ^{D}PG12 as compared to TZ2.

TABLE 3: Simulations of Tetrapeptides, BG4 and BG4-^{D}Val[a]

BG4						BG4-^{D}Val	
300 K		450 K		450 K		450 K	
time duration (ns)	ϕ (sign)[b,c]	time duration (ns)	ϕ (sign)	time duration (ns)	ϕ (sign)	time duration (ns)	ϕ (sign)
0−80	−	0−4	−	0−7	+	0−5.5	−
80−200	+	4−30	+	9−22	−	5.9−28.0	−
		31−67	+	22−37	+	28.5−55.0	+
		68−88	+	39−79	−	57.0−100	−
		89−100	+	81−100	+		
time with + geometry	120		93		41		26.5
time with − geometry	80		4		41		80.6

[a] Transitions between mirror turn vs common turn geometry at ϕ in an Aib residue. Time unit is nanoseconds. [b] +, − signs represent the mirror turn geometry with approximately 60° and the common turn geometry at ϕ with approximately −60° of the Aib residue, respectively. [c] Very short-lived intermediates representing an extended structure with $\phi = 180°$ are not shown, but their existence is indicated when the consecutive periods have the same sign of ϕ values as indicated in one of the trajectories of BG4 at 450 K.

Our results suggest that the mean value of FETs is longer for TZ2 (38.7 ns) than ^{D}PG12 (25.5), but they are not significantly different (Figure 5) and have nearly the same variance, indicating a higher relative divergence of the FET for ^{D}PG12. This may imply that there is a more heterogeneous unfolding mechanism with ^{D}PG12. Snow et al. previously measured unfolding rates and estimated the activation energy for TZ2.[5] If these results are extrapolated to 450 K, the unfolding time is estimated to be 17 or 0.86 ns, depending on the experimental probe used (fluorescence or IR, respectively). Therefore, our estimated FET values are too long, differing by factors of 2−3 or 40, depending on the experimental method used for the comparison. Tracking H-bond breakage most likely is more like the IR sampling than the CD, which samples Trp−Trp interactions. [Here, the high-temperature approximation is made by assuming an Arrhenius behavior to estimate the rate at 450 K.].

Strong Turn Propensity with ^{D}Pro-Gly or Aib-Gly but Not with Asn-Gly. Our results show that the strong propensity to form a mirror β-turn geometry, as observed with Aib-Gly and ^{D}Pro-Gly turn sequences, leads to β-hairpin stability for the two Gellman-like peptide sequences, BG12 and ^{D}PG12. Our atomistic simulations detail how folded state stability benefits from the intrinsic structural characteristics of these turn sequences both in refolding pathways and in unfolding pathways. By contrast, an Asn-Gly turn sequence, though often seen to form tight β-turns in proteins, does not show a strong β-turn propensity in isolation. Rather, Asn residues favor a common turn geometry that adversely destabilizes refolding attempts in hairpins. This is consistent with experimental results that indicate NG12 does not form a stable, well-folded β-hairpin.[13,46] Simulations with PG12 and the tetrapeptide models also provide convincing arguments why β-hairpin formation of two Gellman peptides, BG12 and ^{D}PG12, is facilitated by the turn residues.

By contrast, TZ2, which has an Asn-Gly turn, is a strong β-hairpin folder. As consistent with previous studies,[5,23,24,32,35,64,71] and again revealed in our comparison of the TZ2 trajectory (Figure 2(d) and 3(d)), the strong stabilization effect arises from hydrophobic core interactions among four Trp residues in the strands. This is sufficient to allow the dynamics of the nascent partially folded structure to continue on to the folded state. With TZ2, any negative impact from the Asn-Gly turn, as observed with NG12, could be overcome with the contributions from hydrophobic interactions of the strand side chains.

Finally, we observe that simulations with PG12 and tetrapeptides provide added evidence of the propensity of the turns such as the Aib-Gly or the ^{D}Pro-Gly. The propensity to form a strong mirror-tight turn provides positive impetus for formation of the β-turn structure.

Heterogeneous Folding in Thermal Unfolding IR Experiments. Presumably, if a sigmoidal transition is obtained using data obtained from thermal unfolding experiments, it might be indicative of an underlying two-state process. Our previous thermal unfolding experiments using amide I IR and electronic CD spectroscopies as well as many studies from other groups have shown that tryptophan zipper hairpins such as TZ2 exhibit, at least partially, a sigmoidal transition.[24,32] On the other hand, BG12 and its ^{13}C isotopic variants did not show such a sigmoidal transition.[8,13,23]

Our interpretation is that the absence of sigmoidal transition with two Gellman hairpins is related to pronounced heterogeneous folding dynamics seen in BG12 and ^{D}PG12. Our simulation results, from conformational analyses of the trajectories as well as via PCA analysis, confirm that the Gellman β-hairpin model exploits the strong turn propensity of the ^{D}Pro-Gly and Aib-Gly sequences to enhance the stability of the folded structures beyond the moderate hydrophobic contributions from the strand. Therefore, two independent contributions from the turn and the strands have a complicated interplay. As a result, it is conceivable that folding pathways and unfolding pathways of two Gellman hairpins exhibit various conformational fluctuations depending upon how the two contributions combine, which is exactly what we observed with the *unfolding simulations*. Indeed, the *unfolding simulations* of ^{D}PG12 highlight such complications by showing active conformational fluctuations with short-lived intermediates representing the residual turn structures and strand interactions. In fact, heterogeneous folding dynamics was previously suggested for TZ2 with detection-dependent observations.[35] As shown with our results, the Gellman peptides seem to be an example of an enhanced heterogeneous folding mechanism which is highly likely to be the reason for their lacking a sigmoidal transition.

V. Concluding Remarks

MD simulations employing the all-atom peptide model with explicit water molecules were carried out for elucidating structural origins of the β-hairpin formation of a series of 12-mer peptides, ^{D}PG12, BG12, NG12, and TZ2.

Our main conclusion is that the folded state stability of BG12 and ^{D}PG12 is associated with pronounced contributions from the turn adding to a moderate contribution from cross-strand interactions, which gives rise to a complicated interplay between turn and strand contributions to stability. This is contrast to TZ2 where the folding mechanism is dominated by cross-strand hydrophobic side-chain interactions. Such interplay in folding dynamics of BG12 and ^{D}PG12 explains various experimental observations, such as the hairpin stability accompanied with the

absence of sigmoidal feature in melting experiments. It is argued that underlying pronounced heterogeneous folding pathways provide molecular level interpretations for several experimental observations.

Acknowledgment. This research was funded by grants from the National Science Foundation (CHE03-16014, CHE07-18543). We are grateful for access to the computing resources from the UIC Academic Computing Center and from the Center for Computation and Technology (CCT) of LSU.

Supporting Information Available: Figures S1−S4 and Table S-I. This material is available free of charge via the Internet at http://pubs.acs.org.

References and Notes

(1) Huang, R.; Setnicka, V.; Etienne, M. A.; Kim, J.; Kubelka, J.; Hammer, R. P.; Keiderling, T. A. *J. Am. Chem. Soc.* **2007**, *129*, 13592.
(2) Searle, M. S.; Ciani, B. *Curr. Opin. Struct. Biol.* **2004**, *14*, 458.
(3) Munoz, V.; Henry, E. R.; Hofrichter, J.; Eaton, W. A. *Proc. Natl. Acad. Sci. U.S.A.* **1998**, *95*, 5872.
(4) Godoy-Ruiz, R.; Henry, E. R.; Kubelka, J.; Hofrichter, J.; Munoz, V.; Sanchez-Ruiz, J. M.; Eaton, W. A. *J. Phys. Chem. B* **2008**, *112*, 5938.
(5) Snow, C. D.; Qiu, L.; Du, D.; Gai, F.; Hagen, S. J.; Pande, V. S. *Proc. Natl. Acad. Sci. U.S.A.* **2004**, *101*, 4077.
(6) Cochran, A. G.; Skelton, N. J.; Starovasnik, M. A. *Proc. Natl. Acad. Sci. U.S.A.* **2001**, *98*, 5578.
(7) Dyer, R. B.; Maness, S. J.; Peterson, E. S.; Franzen, S.; Fesinmeyer, R. M.; Andersen, N. H. *Biochemistry* **2004**, *43*, 11560.
(8) Hilario, J.; Kubelka, J.; Syud, F. A.; Gellman, S. H.; Keiderling, T. A. *Biospectroscopy* **2002**, 233.
(9) Gellman, S. H. *Curr. Opin. Struct. Biol.* **1998**, *2*, 717.
(10) Galzitskaya, O. V.; Higo, J.; Finkelstein, A. V. *Curr. Protein Pept. Sci.* **2002**, *3*, 191.
(11) Keiderling, T. A. *Curr. Opin. Chem. Biol.* **2002**, *6*, 682.
(12) Gnanakaran, S.; Hochstrasser, R. M.; Garcia, A. E. *Proc. Natl. Acad. Sci. U.S.A.* **2004**, *101*, 9229.
(13) Hilario, J.; Kubelka, J.; Keiderling, T. A. *J. Am. Chem. Soc.* **2003**, *125*, 7562.
(14) Griffiths-Jones, S. R.; Maynard, A. J.; Searle, M. S. *J. Mol. Biol.* **1999**, *292*, 1051.
(15) Ferguson, N.; Fersht, A. R. *Curr. Opin. Struct. Biol.* **2003**, *13*, 75.
(16) Dinner, A. R.; Lazaridis, T.; Karplus, M. *Proc. Natl. Acad. Sci. U.S.A.* **1999**, *96*, 9068.
(17) Klimov, D. K.; Thirumalai, D. *Proc. Natl. Acad. Sci. U.S.A.* **2000**, *97*, 2544.
(18) Setnicka, V.; Huang, R.; Thomas, C. L.; Etienne, M. A.; Kubelka, J.; Hammer, R. P.; Keiderling, T. A. *J. Am. Chem. Soc.* **2005**, *127*, 4992.
(19) Kim, J.; Huang, R.; Kubelka, J.; Bour, P.; Keiderling, T. A. *J. Phys. Chem. B* **2006**, *110*, 23590.
(20) Kubelka, J.; Keiderling, T. A. *J. Am. Chem. Soc.* **2001**, *123*, 6142.
(21) Ludlam, C. F. C.; Arkin, I. T.; Liu, X. M.; Rothman, M. S.; Rath, P.; Aimoto, S.; Smith, S. O.; Engelman, D. M.; Rothschild, K. J. *Biophys. J.* **1996**, *70*, 1728.
(22) Decatur, S. M.; Antonic, J. *J. Am. Chem. Soc.* **1999**, *121*, 11914.
(23) Hauser, K.; Krejtschi, C.; Huang, R.; Wu, L.; Keiderling, T. A. *J. Am. Chem. Soc.* **2008**, *130*, 2984.
(24) Huang, R.; Wu, L.; McElheny, D.; Bour, P.; Roy, A.; Keiderling, T. A. *J. Phys. Chem. B* **2009**, *113*, 5661.
(25) Ganim, Z.; Chung, H. S.; Smith, A. W.; Deflores, L. P.; Jones, K. C.; Tokmakoff, A. *Acc. Chem. Res.* **2008**, *41*, 432.
(26) Wang, J.; Chen, J.; Hochstrasser, R. M. *J. Phys. Chem. B* **2006**, *110*, 7545.
(27) Kim, Y. S.; Liu, L.; Axelsen, P. H.; Hochstrasser, R. M. *Proc. Natl. Acad. Sci. U.S.A.* **2008**, *105*, 7720.
(28) Kubelka, J.; Bour, P.; Keiderling, T. A. Quantum Mechanical Calculations of Peptide Vibrational Force Fields and Spectral Intensities. In *Advances in Biomedical Spectroscopy, Vol. 2, Biological and Biomedical Infrared Spectroscopy*; Barth, A., Haris, P. I., Eds.; IOS Press: Amsterdam, 2009; Vol. 2, p 178.
(29) Kubelka, J.; Keiderling, T. A. *J. Phys. Chem. A* **2001**, *105*, 10922.
(30) Bour, P.; Keiderling, T. A. *J. Phys. Chem. B* **2005**, *109*, 232687.
(31) Bour, P.; Sopkova, J.; Bednarova, L.; Malon, P.; Keiderling, T. A. *J. Comput. Chem.* **1997**, *18*, 646.
(32) Wu, L.; McElheny, D.; Huang, R.; Keiderling, T. A. *Biochemistry* **2009**, *48*, 10362.
(33) Hughes, R. M.; Waters, M. L. *Curr. Opin. Struct. Biol.* **2006**, *16*, 514.
(34) Smith, A. W.; Chung, H. S.; Ganim, Z.; Tokmakoff, A. *J. Phys. Chem. B* **2005**, *109*, 17025.
(35) Yang, W. Y.; Pitera, J. W.; Swope, W. C.; Gruebele, M. *J. Mol. Biol.* **2004**, *336*, 241.
(36) Du, D.; Zhu, Y.; Huang, C.; Gai, F. *Proc. Natl. Acad. Sci. U.S.A.* **2004**, *101*, 15915.
(37) Syud, F. A.; Stanger, H. E.; Gellman, S. H. *J. Am. Chem. Soc.* **2001**, *123*, 8667.
(38) Chebaro, Y.; Dong, X.; Laghaei, R.; Derreumaux, P.; Mousseau, N. *J. Phys. Chem. B* **2009**, *113*, 267.
(39) Chen, C.; Xiao, Y. *Bioinformatics* **2008**, *24*, 659.
(40) Yang, L.; Shao, Q.; Gao, Y. Q. *J. Phys. Chem. B* **2009**, *113*, 803.
(41) Bonomi, M.; Branduardi, D.; Gervasio, F. L.; Parrinello, M. *J. Am. Chem. Soc.* **2008**, *130*, 13938.
(42) Wei, G.; Mousseau, N.; Derreumaux, P. *Proteins: Struct., Funct., Bioinf.* **2004**, *56*, 464.
(43) Imamura, H.; Chen, J. Z. Y. *Proteins: Struct., Funct., and Bioinf.* **2006**, *63*, 555.
(44) Butterfield, S. M.; Sweeney, M. M.; Waters, M. L. *J. Org. Chem.* **2005**, *70*, 1105.
(45) Robinson, J. A. *Acc. Chem. Res.* **2008**, *41*, 1278.
(46) Stanger, H. E.; Gellman, S. H. *J. Am. Chem. Soc.* **1998**, *120*, 4236.
(47) Ragothama, S. R.; Awasthi, S. K.; Balaram, P. *J. Chem. Soc., Perkin Trans.* **1998**, *2*, 137.
(48) Nagaraj, R.; Shamala, N.; Balaram, P. *J. Am. Chem. Soc.* **1979**, *101*, 16.
(49) Thomas, C. L.; Etienne, M. A.; Wang, J.; Setnicka, V.; Keiderling, T. A.; Hammer, R. P. In Peptide revolution: genomics, proteomic, and therapeutics. *The 18th American peptide society meeting*, San diego, 2004.
(50) Zhang, J.; Qin, M.; Wang, W. *Proteins: Struct., Funct., Bioinform.* **2006**, *62*, 672.
(51) Lindahl, E.; Hess, B.; Spoel, D. v. d. *J. Mol. Model.* **2001**, *7*, 306.
(52) Jorgensen, W.; Maxwell, D. S.; Tirado-Rives, J. *J. Am. Chem. Soc.* **1996**, *118*, 11225.
(53) Syud, F. A.; Espinosa, J. F.; Gellman, S. H. *J. Am. Chem. Soc.* **1999**, *121*, 11577.
(54) DeLano. *PyMOL*, 0.99 ed.; DeLano Scientific LLC, 2006.
(55) Zhou, Y.; Zhang, C.; Stell, G.; Wang, J. *J. Am. Chem. Soc.* **2003**, *125*, 6300.
(56) Yang, S.; Kim, J.; Lee, S. *J. Chem. Phys.* **1999**, *111*, 10119.
(57) Amadei, A.; Linssen, A. B. M.; Berendsen, H. J. C. *Proteins: Struct., Funct., Genet.* **1993**, *17*, 412.
(58) Kramers, H. A. *Physica* **1940**, *7*, 284.
(59) Tai, K. *Biophys. Chem.* **2004**, *107*, 213.
(60) Smith, L. J.; Daura, X.; Gunsteren, W. F. v. *Proteins: Struct. Funct., Genet.* **2002**, *48*, 10.
(61) Hansson, T.; Oostenbrink, C.; Gunsteren, W. F. v. *Curr. Opin. Struct. Biol.* **2002**, *12*, 7.
(62) Lei, H.; Duan, Y. *Curr. Opin. Struct. Biol.* **2007**, *17*, 187.
(63) Settanni, G.; Fersht, A. *Biophys. J.* **2008**, *94*, 4444.
(64) Nymeyer, H. *J. Phys. Chem. B* **2009**, *113*, 8288.
(65) Kim, J.; Kapitan, J.; Lakhani, A.; Bour, P.; Keiderling, T. A. *Theor. Chem. Acc.* **2008**, *119*, 81.
(66) Zhou, H.-X.; Szabo, A. *Biophys. J.* **1996**, *71*, 2440.
(67) Caves, L. S. D.; Evanseck, J. D.; Karplus, M. *Proteins Sci.* **1997**, *7*, 649.
(68) Auffinger, P.; Westhof, E. *Biophys. J.* **1996**, *71*, 940.
(69) Zhou, R.; Berne, B. J. *Proc. Natl. Acad. Sci. U.S.A.* **2002**, *99*, 12777.
(70) Szabo, A.; Schulten, K.; Schulten, Z. *J. Chem. Phys.* **1980**, *72*, 4350.
(71) Takekiyo, T.; Wu, L.; Yoshimura, Y.; Shimizu, A.; Keiderling, T. A. *Biochemistry* **2009**, *48*, 1543.

JP912159T